Dynamic study of a roller bearing in a planetary application considering the hydrodynamic lubrication of the roller/cage contact

M. Denni, N. Biboulet, V. Abousleiman, A.A. Lubrecht

Version of Record: https://www.sciencedirect.com/science/article/pii/S0301679X19301744
Manuscript_bf1fbe93459ba9f436306f0d4b2b48d0

Dynamic Study of a Roller Bearing in a Planetary Application considering the Hydrodynamic Lubrication of the Roller/Cage Contact.

M. Denni[a,b,*], N. Biboulet[a], V. Abousleiman[b], A.A. Lubrecht[a]

[a] *Université de Lyon, INSA-Lyon, CNRS UMR 5259,* LaMCoS, *Villeurbanne F-69621, France*
[b] *SAFRAN Transmission Systems, 18 Bvd L. Seguin, 92707 Colombes, France*

Abstract

A new multi-body dynamics model for the simulation of roller bearings in planetary applications is presented. Analytical relations are used to model the lubricated contacts involved in the bearing. In particular, the vertical damping of the oil film in the roller/cage contact is taken into account, in order to get an accurate estimation of the forces endured by the cage. Results are presented for the case of a planet gear roller bearing in a turbofan planetary gearbox in terms of roller/ring and roller/cage forces and their influence on the instantaneous cage speed. The flexibility of the outer ring is also modelled using a finite element model; its influence on the results, i.e. on the maximum roller/ring force and on the bearing dynamics, is presented.

Keywords: Roller bearing, dynamic behavior, planetary applications, centrifugal field, roller/cage impact.

Notation

E'	Reduced modulus of elasticity [Pa]
F	Resulting force on element [N]
F_p	Dimensionless Poiseuille viscous force per unit length [−]
f_p	Poiseuille viscous force per unit length [$\mathrm{N\,m^{-1}}$]
G	Resulting moment on element [N m]
h	Film thickness [m]
H_m	Dimensionless minimum film thickness [−]
h_m	Minimum film thickness [m]
I	Element moment of inertia [$\mathrm{kg\,m^2}$]
L	Dimensionless material parameter [−]
m	Element mass [kg]
M_1	Dimensionless load parameter per unit-length [−]
p	Pressure [Pa]
R	Contact radius [m]
r	Element radial position [m]
R_c	Carrier radius [m]
t	Time [s]
U	Dimensionless speed parameter [−]
u_m	Fluid entrainment velocity [$\mathrm{m\,s^{-1}}$]
w_1	Load carrying capacity per unit-length [$\mathrm{N\,m^{-1}}$]
x	Horizontal axis coordinate [m]
x_1	Element horizontal position [m]
y_1	Element vertical position [m]

*Corresponding author: martin.denni@insa-lyon.fr

α	Piezo-viscosity coefficient [Pa^{-1}]
Δ	Gap separating bodies (undeformed geometry) [m]
δ	Contact elastic deformation [m]
η_0	Dynamic viscosity [Pa s]
ψ	Carrier rotation angle [rad]
θ	Element angular position [rad]
φ	Element rotation angle [rad]

Subscripts

$_r$	Radial direction
$_x$	Horizontal direction
$_y$	Vertical direction
$_\theta$	Tangential direction

1. Introduction

In roller bearings, the cage is used as a separator to prevent rolling elements to contact and it is usually not designed to support high loads. However, in some applications such as planetary gearboxes, the entire bearing is rotating around an axis inducing centrifugal forces on all its elements. In such a case, high friction losses are observed and cracks sometimes initiate leading to cage failure. This last observation suggests that high forces are encountered in the contact between the rollers and the cage.

Since the 1970s, many numerical models for the study of the dynamic behavior of roller bearings have been developed. One of the most famous ones is the ADORE code developed by Gupta [1]. The same author also published a complete literature review [2] on rolling bearing modeling. The work by Harris [3] remains a reference in the world of rolling bearing and many topics are covered in his book. Nevertheless, the number of published papers on roller bearings working under a centrifugal field is very limited. The only known work is by Houpert [4] [5] who developed the code CAGEDYN for the study of the dynamics of a roller bearing in a planetary application. The focus is on the roller/cage contact and the roller radial position is defined using a quasi-static approach for the roller/ring contact. This enables one to limit the CPU time. Furthermore, in his work a dry contact law is chosen for the roller/cage contact allowing one to compute an equivalent contact stiffness and simplify the problem. However, this does not permit to account for the lubrication of the contact and oil film energy dissipation can not be computed.

Roller bearings almost always work under lubricated conditions. Both hydrodynamic (HD) and elasto-hydrodynamic (EHD) lubrication regimes are thus encountered in these applications. The hydrodynamic normal and viscous force expressions can be obtained analytically using simple geometries. Furuhama [6] was the first to publish his work on the hydrodynamic contact accounting for the squeeze film dissipation in addition to the classical rolling motion. Concerning the EHD contact, forces can not be expressed analytically; it is usual practise to compute the pressure distribution numerically and the contact forces by integration of the pressure field. However, for the sake of efficiency, analytical expressions of the forces should be preferred in dynamic models. Biboulet and Houpert [7] did a numerical study of the EHD pure rolling contact in fully flooded conditions and presented curve fitted equations of the contact forces. This allows one to obtain analytical expressions that can be quickly evaluated in a dynamic model.

The flexibility of the rings can influence the size of the bearing loaded zone, especially in aeronautics where lightened components are used. Thus it is important to take this effect into account. Jones and Harris [8] presented an analytical quasi-static model to compute the deformation of a planet gear. Nevertheless, this model is only valid for symmetric loading and cannot be used in a dynamic solver with a time-varying load. The finite element method (FEM) is also an option to model the flexibility of the outer ring. However, it usually requires many nodes to accurately account for the local contact deformation. Therefore, the local contact deformation is usually removed from the FEM model and computed analytically, allowing to considerably reduce the number of nodes. Wensing [9] developed a semi-analytical model of the flexibility of a bearing housing using FEM and the Ritz method consisting in expressing the ring deformation as a combination of shape functions. In the same way, Leblanc *et al.* [10] developed a dynamic model accounting for the flexibility of the rings using Fourrier series to describe the rings out-of-roundness. Another semi-analytical approach has also been developed by Fiszer *et al.* [11].

The present paper introduces a new roller bearing model for planetary applications such as the planetary gearbox in geared turbofans. The aim of this work is to precisely understand how the centrifugal acceleration induces abnormally high forces on the cage. In order to maintain reasonable computation times, accurate and efficient contact laws are used with a two-dimensional model.

2. Theory

The model presented hereby is a multi-body dynamics model: the equations of motion are solved for each of the roller bearing elements with a given number of degrees of freedom. Contact laws are then chosen to model every contact and compute interaction forces and deformations.

2.1. Equations of motion

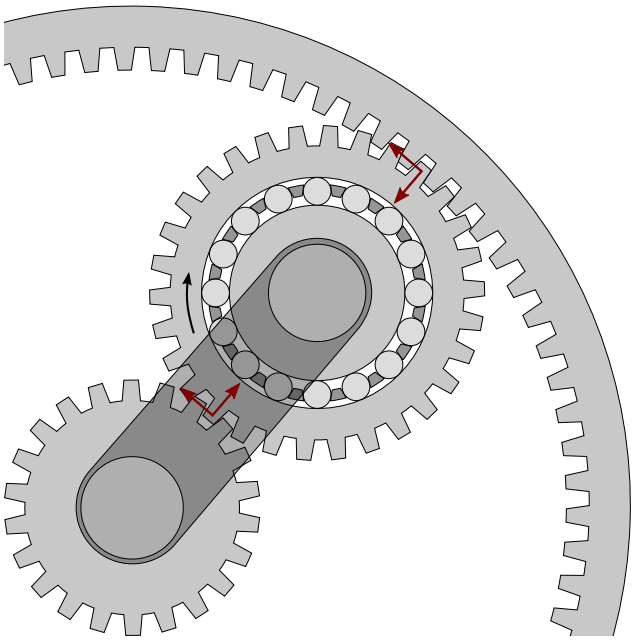

Figure 1: Planetary gear train scheme

The present paper aims at modelling a roller bearing linking the planet gear to the carrier of a planetary gear train. The system is presented in figure 1. Note that only the roller bearing of the planet is represented. Moreover, one can observe that the roller bearing outer ring is also the planet gear; its rotating speed is imposed and its meshing with the sun and the ring gears are modelled as a boundary conditions in terms of forces which are represented in the figure. The problem is solved in two dimensions: the inner ring is fixed, the outer ring has 2 degrees of freedom – two translations –, the rolling elements have 3 degrees of freedom – two translations and one rotation –, the cage is guided by the inner ring and only has one rotational degree of freedom. The cage bridges – i.e the cage pins separating the rolling elements – are considered flexible with respect to the cage bulk and also have one degree of freedom to describe their angular position.

Figure 2 presents the different reference frames of the system. The equations of motion are expressed in the bearing reference frame and can be written as follows:

$$m\frac{\partial^2 x_1}{\partial t^2} = F_x + m\left(y_1\frac{\partial^2\psi}{\partial t^2} + (R_c + x_1)\left(\frac{\partial\psi}{\partial t}\right)^2 + 2\frac{\partial\psi}{\partial t}\frac{\partial y_1}{\partial t}\right) \tag{1}$$

$$m\frac{\partial^2 y_1}{\partial t^2} = F_y - m\left((R_c + x_1)\frac{\partial^2\psi}{\partial t^2} - y_1\left(\frac{\partial\psi}{\partial t}\right)^2 + 2\frac{\partial\psi}{\partial t}\frac{\partial x_1}{\partial t}\right) \tag{2}$$

$$I\frac{\partial^2\varphi}{\partial t^2} = G_z \tag{3}$$

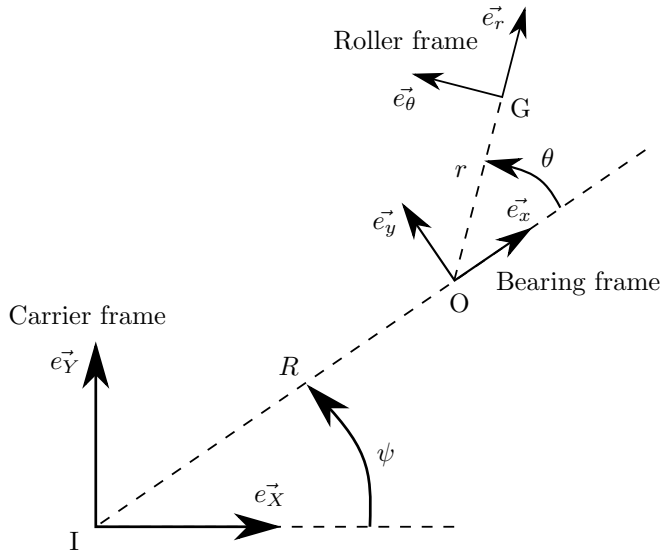

Figure 2: Reference frames

As the bearing frame is not an inertial reference frame, the centrifugal forces due to its rotation over the z-axis of the carrier frame are included in the previous expressions.

The last expressions of the equations of motions are used to compute the acceleration of the outer ring. However, the rollers are easier to follow with their radial and angular positions, velocities and accelerations. Therefore, the equations of motion are also written in the cylindrical coordinate system:

$$m\frac{\partial^2 r}{\partial t^2} = F_r - m\left[R_c \sin\theta \frac{\partial^2 \psi}{\partial t^2} - R_c \cos\theta \left(\frac{\partial \psi}{\partial t}\right)^2 - r\left(\frac{\partial \psi}{\partial t} + \frac{\partial \theta}{\partial t}\right)^2\right] \tag{4}$$

$$mr\frac{\partial^2 \theta}{\partial t^2} = F_\theta - m\left[(r + R_c \cos\theta)\frac{\partial^2 \psi}{\partial t^2} + R_c \sin\theta \left(\frac{\partial \psi}{\partial t}\right)^2 + 2\frac{\partial r}{\partial t}\left(\frac{\partial \psi}{\partial t} + \frac{\partial \theta}{\partial t}\right)\right] \tag{5}$$

$$I\frac{\partial^2 \varphi}{\partial t^2} = G_z \tag{6}$$

The previous equations are solved at every time-step using an implicit second order Newmark scheme and a Newton-Raphson algorithm. The time-step is variable and automatically adapts to ensure a constant discretisation error.

2.2. Lubricated contacts

2.2.1. Roller/cage contact

Contacts between the rollers and the cage are the key issue of the present model. Indeed impacts must be accurately accounted for to allow a proper study of the dynamics of the cage. As said in the previous section, the cage bridges have their own stiffness with respect to the cage bulk. This stiffness, computed using an analytical beam model, is a first important step to represent the contact details. Figure 3 shows the gap separating the roller from the bridge and the contact load with respect to the impact time under dry contact conditions. One can observe that one single impact under dry conditions is in fact composed of multiple smaller impacts because of the bridge flexibility and the high stiffness of the dry contact.

Another step towards a more realistic model for this contact is to consider the oil lubrication. Pressure in the roller/cage contact is supposed to be low enough to neglect elastic deformation. Thus a hydrodynamic lubrication regime is considered. With the assumption that the fluid is incompressible, the Reynolds equation governing the pressure p and film thickness h in a lubricated line contact is given by:

$$\frac{\partial}{\partial x}\left(\frac{h^3}{12\eta_0}\frac{\partial p}{\partial x}\right) - u_m \frac{\partial h}{\partial x} = \frac{\partial h}{\partial t} \tag{7}$$

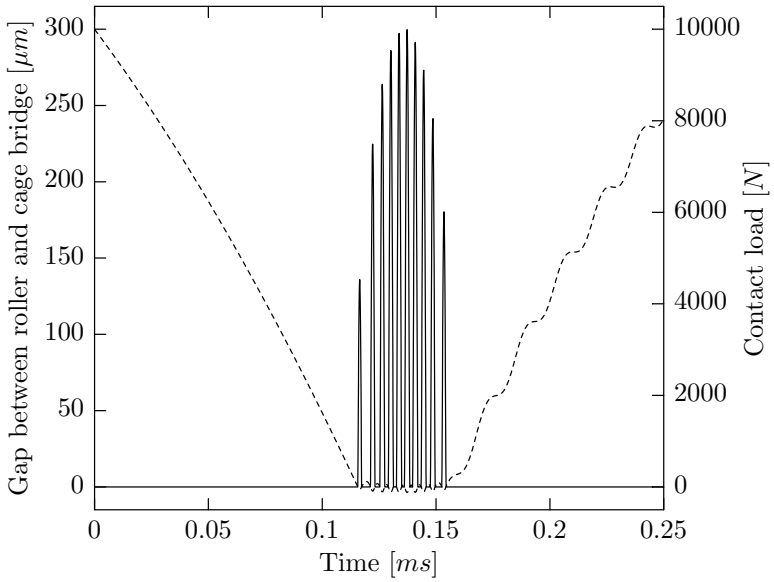

Figure 3: Gap between roller and cage bridge (dashed line) and contact load (solid line) during impact under dry contact conditions.

Assuming a parabolic geometry for the bodies in contact, this equation has been solved semi-analytically. The right hand side is the derivative of the film thickness with respect to time, i.e. the impact speed of the bodies. Finally, one obtains the semi-analytical expressions of the normal force and the Poiseuille and Couette viscous forces with respect to the minimum film thickness, i.e. the gap between bodies, and the impact speed. This allows a quick and accurate evaluation of the contact forces.

Figure 4 shows the same impact as figure 3 but under hydrodynamic lubrication conditions. It can be noticed that in this case, only one peak appears. Furthermore, the maximum force is lower because of the vertical damping of the oil film. Energy dissipation occurs in the oil film which can be observed by comparing the gap increase speed between the dry and the lubricated case after the impact.

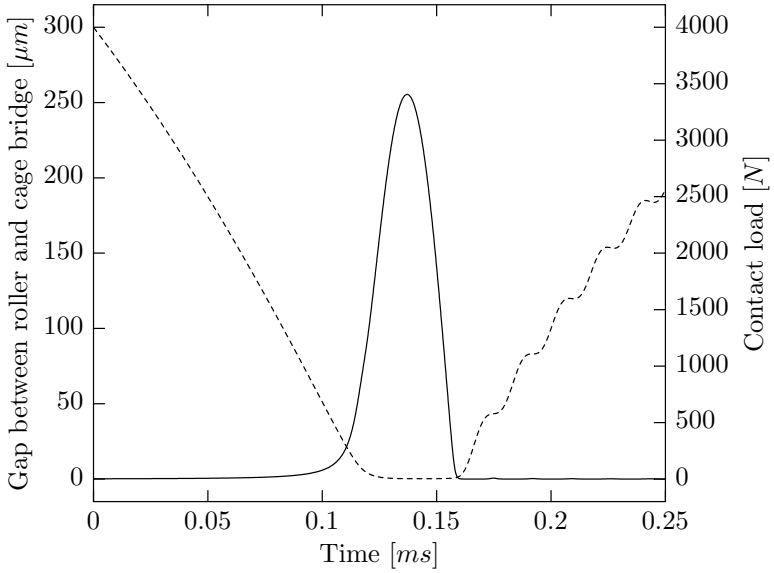

Figure 4: Gap between roller and cage bridge (dashed line) and contact load (solid line) during impact under hydrodynamic contact conditions.

2.2.2. Roller/ring contact

Lubrication is also considered in the roller/ring contact in order to have a good approximation of the viscous losses. The pressure induced in this contact is much higher than in the roller/cage contact. Thus

elastic deformations can not be neglected and this contact works under the elasto-hydrodynamic (EHD) lubrication regime.

Introducing the speed parameter $U = 2\eta u_m/(E'R)$ and using the film thickness equation proposed by Moes [12], one can express the load parameter $M_1 = w_1/(E'R\sqrt{U})$ with respect to the dimensionless minimum film thickness $H_m = h_m/(R\sqrt{U})$ and the material parameter $L = \alpha E' \sqrt[4]{U}$ in the piezo-viscous elastic (PVE) and in the iso-viscous rigid (IVR) regime. These expressions are a curve-fit of numerical results for stationary EHD line contact:

$$M_1 = L^6 \left(\frac{1.31}{H_m}\right)^8 \quad \text{(PVE)} \tag{8}$$

$$M_1 = \frac{3}{H_m} \quad \text{(IVR)} \tag{9}$$

Having the positions of the bearing elements, one can calculate the gap Δ separating the rollers from the rings with the undeformed geometry. In the IVR regime, illustrated in figure 5a, no elastic deformation occurs and the oil fills the gap since fully flooded conditions are assumed. Thus the film thickness is equal to the gap. In the PVE regime, illustrated in figure 5b, an elastic deformation δ will occur and the minimum film thickness is in fact larger than the gap previously calculated. The film thickness has to be computed such that the Hertzian force and the load carrying capacity of the film are equal. For that purpose an algorithm has been implemented to determine the working regime and the minimum film thickness using the gap and the entrainment speed.

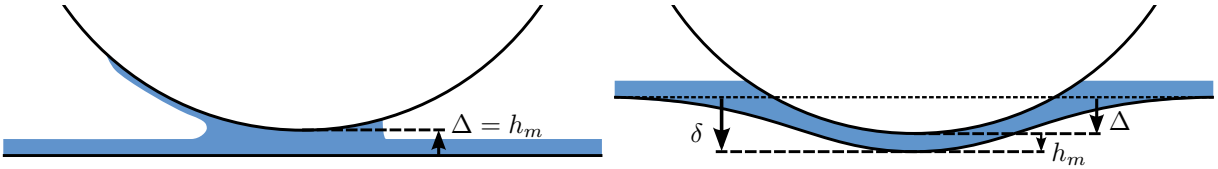

(a) no elastic deformation (IVR) (b) significant elastic deformation (PVE)

Figure 5: Contact lubrication under IVR and PVE regimes

Two kinds of viscous forces, i.e. tangential contact forces, coexist in the contact: the Couette force which depends on the speed difference between the bodies – i.e. the sliding speed, and the Poiseuille force coming from the pressure gradient in the oil film and depending on the entrainment velocity. The Couette force is computed using a simple friction law: it is nil for pure rolling conditions and increases linearly with the slide-to-roll ratio until the maximum friction force.

When high sliding occurs, the Poiseuille force is very small compared to the Couette force. However, in the case of low sliding speeds close to pure rolling contact conditions the Poiseuille force is significant. Therefore it is computed only for pure-rolling conditions. Using the work of Biboulet and Houpert [7], the dimensionless Poiseuille viscous force per unit-length $F_p = f_p/(E'R)$ for pure rolling contacts and fully flooded conditions can be written with respect to the load and speed parameters for the IVR and PVE regimes:

$$F_p = \begin{cases} 1.42\, U^{0.75} M_1^{0.5} & \text{if } M_1 < 1.07 \text{ (IVR)} \\ 1.47\, U^{0.75} & \text{otherwise (PVE)} \end{cases} \tag{10}$$

Note that F_p in the PVE regime is constant and does not depend of the contact normal force.

2.3. Flexible outer ring

The flexibility of the outer ring influences the size of the loaded zone and the number of rollers supporting the load. Thus the dynamics of the entire bearing can be highly influenced by the outer ring out-of-roundness and it should be considered when computing the roller/outer ring forces.

Assuming that the deformation speed of the outer ring is important compared to the roller frequency, the dynamic effects on the outer ring are neglected and a quasi-static model is developed. A FEM model of the ring is created using an external tool in order to obtain the stiffness matrix of the outer ring raceway. The stiffness matrix is then condensed on the nodes of the raceway and reversed to get the flexibility matrix. Furthermore, the contribution of local deformation is removed by computing the stiffness matrix of a ring completely clamped on the outer surface and subtracting it to the stiffness matrix of the ring. Finally, an algorithm is developed to balance the rollers forces with the ring deformation.

3. Results

The simulations have been conducted for a typical planet gear roller bearing geometry. The carrier rotating speed is set to 3 000 rpm and the planet gear speed is 10 000 rpm. Under these conditions, the centrifugal force applied on the outer ring is approximately 45 000 N. A gear load of 10 000 N is also applied on the outer ring. The results are first presented for a rigid outer ring. In a second part, the influence of the flexibility of the outer ring is studied.

3.1. Rigid outer ring

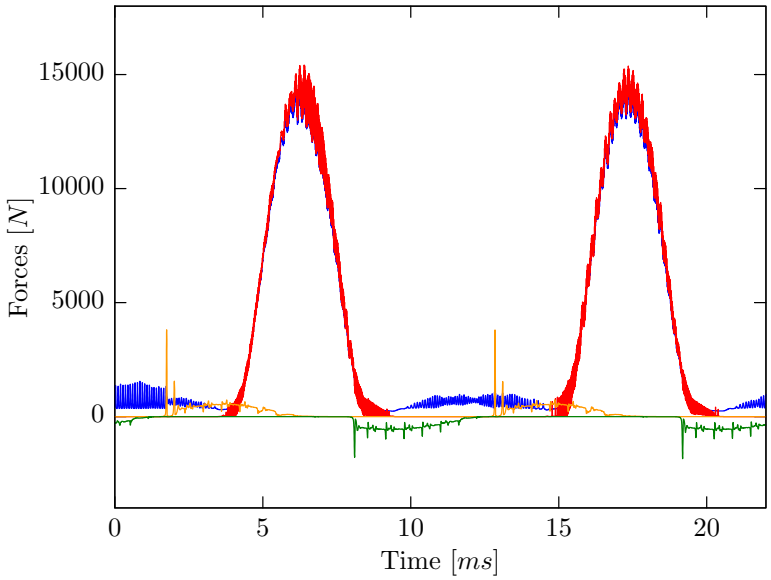

Figure 6: Forces on a roller during two bearing rotations: red and blue lines – inner and outer ring forces, yellow and green lines – rear and front bridge forces.

Results are presented in figure 6 in terms of the forces seen by a roller during its rotation around the bearing. A first observation is to notice the loaded zone where the roller is pinched between the inner and outer ring and thus where the roller/ring forces are increasing. Secondly, one can note the impacts on the cage bridges and their high amplitude which is approximately 3 800 N, more than a quarter of the roller/ring maximum force. Another simulation has been launched for the same roller bearing in a classical case without the centrifugal field. In this case the roller/bridge maximum force never exceeds 100 N. This means that the forces endured by the cage in a planetary application can be up to 40 times higher than for a classical case. This can explain why the cage fails for a bearing working under those high centrifugal force conditions.

The same results are presented using the polar coordinate system in figure 7. The forces are plotted with respect to the angular position of the roller in the bearing reference frame. Note that the rollers are rotating in the clockwise direction. The centrifugal force applied to the outer ring is oriented to the right and the gear resulting force upwards.

The first impact appears at the exit of the loaded zone while the second impact happens on the opposite side. After the impact, the roller/bridge force remains high, approximately 500 N. This can be explained as the centrifugal force on the rollers is pushing them towards the cage. In the 15-135° interval rollers are thus pushing the cage into rotation whereas in the 230-340° interval they resist the cage rotation. Furthermore, one can observe that the two impacts are not perfectly aligned and the impact on the rear bridge is higher; this is because the loaded zone prevents the rollers from accelerating in the cage pocket, delaying and limiting the roller/bridge impact.

Apart from the impact peak, other peaks can be observed in the roller/bridge force. These peaks are caused by the impacts of the other rollers on the cage. It implies that the instantaneous cage speed is affected by all impacts. This is shown in figure 8: the same pattern is repeated every time a pair of rollers impacts the cage. In the present case the bearing is composed of 18 rollers. The figure brings out 3 similar patterns in the cage speed during approximately 2 ms which corresponds to 60° of a roller revolution. The force on one particular cage bridge is also plotted and every main impact on the cage is depicted by a vertical dotted line. One can observe that the first impact on the bridge generates the main peak in the cage speed.

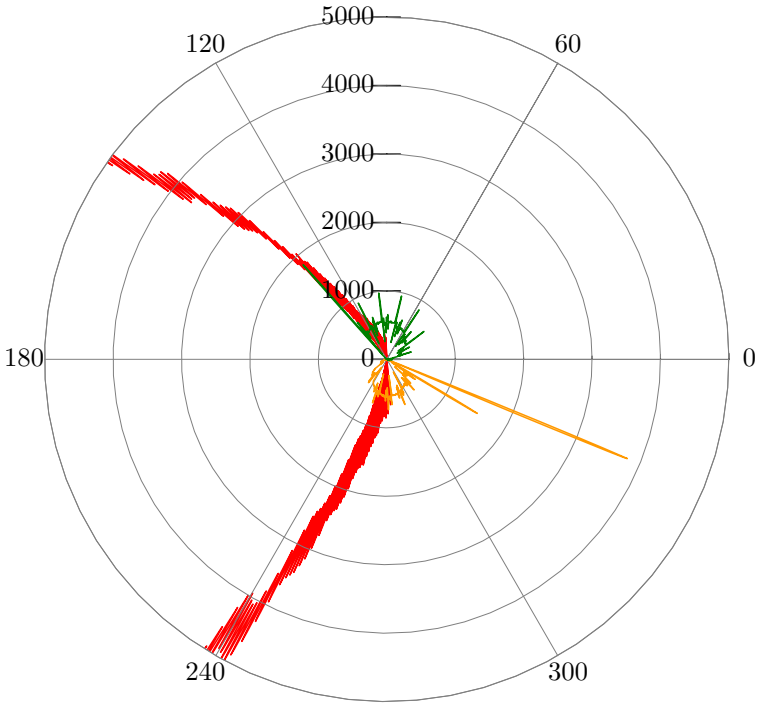

Figure 7: Forces on a roller during one bearing rotation: red line – inner ring force, yellow and green lines – rear and front bridge forces.

The impact on the opposite bridge corresponding to the second vertical line also causes a peak, but in the opposite direction. The impacts on the following bridges influence the cage speed in a similar way making the instantaneous cage speed periodic.

3.2. Flexible outer ring

The same simulation has been launched accounting for the outer ring deformation. The results are presented on figure 9. One can first observe that the width of the loaded zone increases. Therefore, the number of rollers supporting the load increases and the maximum force between roller and rings is reduced.

Another interesting observation is that there is only one instead of two impact peaks between the roller and the cage. The loaded zone being wider, the roller is not free to accelerate when it comes into contact with the front cage bridge and thus it prevents the impact from happening. This phenomenon depends on the flexibility of the ring, which defines the width of the loaded zone, but also on the ratio between the gear resulting force and the centrifugal force applied on the ring. Indeed, this ratio defines the angular position of the loaded zone.

4. Conclusion

In conclusion, a roller bearing model has been developed allowing a better understanding of the dynamics of roller bearings in planetary applications. Special attention has been given to the roller/cage contact to accurately account for the hydrodynamic lubrication of the contact and the energy dissipation of the oil film.

For the case where the outer ring is considered rigid, the results demonstrate that the cage bridges are enduring two very large impacts per revolution, that are comparable to the roller/ring forces. Under these conditions, a classical cage will certainly fail as it is not designed to withstand such high forces.

The outer ring flexibility influences the loaded zone size. This affects the roller bearing dynamics as it can absorb one impact per revolution and limit the cage fatigue for planetary applications.

Finally, a more detailed study of the influence of the geometry parameters, especially of the clearance of the roller in the cage pocket, as well as the oil viscosity or material parameters on the results should be conducted.

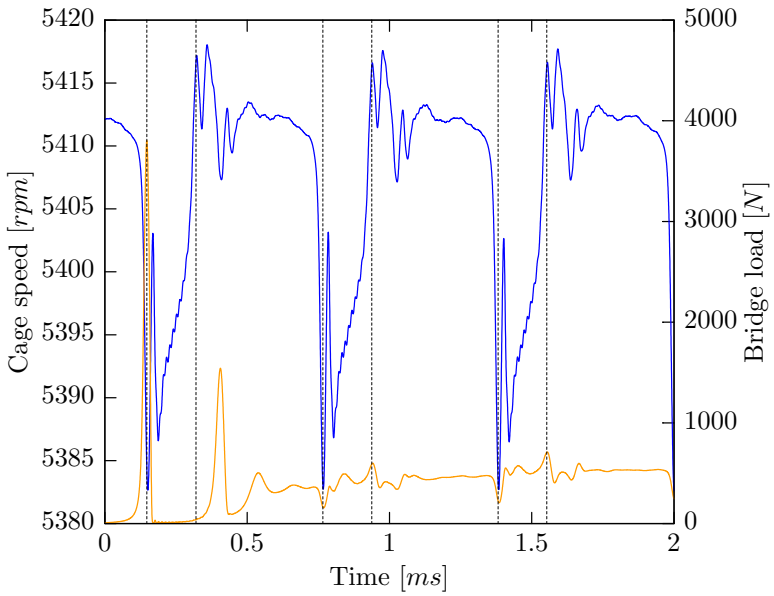

Figure 8: Cage speed (blue) and bridge load (yellow) during approximately 60° of a bearing rotation.

Acknowledgement

The first author would like to thank SAFRAN Transmission Systems for their permission to publish this work.

References

[1] P. K. Gupta, *Advanced Dynamics of Rolling Elements*. Springer-Verlag, 1984.

[2] P. K. Gupta, "Current status of and future innovations in rolling bearing modeling," *Tribology Transactions*, vol. 54, pp. 394–403, 2011.

[3] T. A. Harris, *Rolling Bearing Analysis, Fourth Edition*. John Wiley & Sons, Inc., 2001.

[4] L. Houpert, "Cagedyn: A contribution to roller bearing dynamic calculations part i: Basic tribology concepts," *Tribology Transactions*, vol. 53, pp. 1–9, 2010.

[5] L. Houpert, "Cagedyn: A contribution to roller bearing dynamic calculations part ii: Description of the numerical tool and its outputs," *Tribology Transactions*, vol. 53, pp. 10–21, 2010.

[6] S. Furuhama, "A dynamic theory of piston-ring lubrication: 1st report, calculation," *Bulletin of JSME*, vol. 2, no. 7, pp. 423–428, 1959.

[7] N. Biboulet and L. Houpert, "Hydrodynamic force and moment in pure rolling lubricated contacts. part 1: line contacts," *Proceedings of the Institution of Mechanical Engineers, Part J: Journal of Engineering Tribology*, vol. 224, no. 8, pp. 765–775, 2010.

[8] A. B. Jones and T. A. Harris, "Analysis of a rolling-element idler gear bearing having a deformable outer-race structure," *Journal of Basic Engineering*, vol. 85, no. 2, pp. 273–278, 1963.

[9] J. A. Wensing, *On the dynamics of ball bearings*. PhD thesis, University of Twente, 1998.

[10] A. Leblanc, D. Nelias, and C. Defaye, "Nonlinear dynamic analysis of cylindrical roller bearing with flexible rings," *Journal of Sound and Vibration*, vol. 325, no. 1, pp. 145–160, 2009.

[11] J. Fiszer, T. Tamarozzi, and W. Desmet, "A semi-analytic strategy for the system-level modelling of flexibly supported ball bearings," *Meccanica*, vol. 51, no. 6, pp. 1503–1532, 2016.

[12] H. Moes, *Lubrication and Beyond*. Twente University Press, 2000.

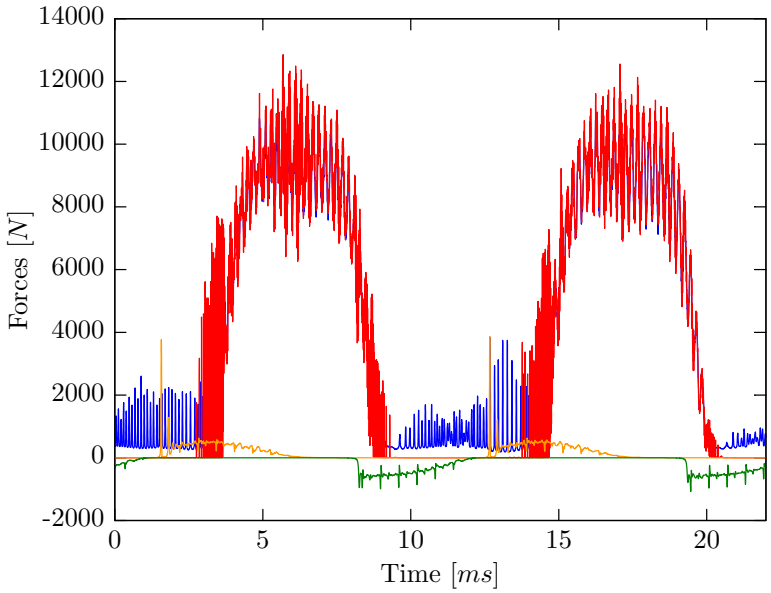

Figure 9: Forces on a roller during two bearing rotations: red and blue lines – inner and outer ring forces, yellow and green lines – rear and front bridge forces.